Density matrix renormalization group calculations on relative energies of transition metal complexes and clusters

Konrad H. Marti, Irina Malkin Ondík, Gerrit Moritz, and Markus Reiher[a)]
Laboratorium für Physikalische Chemie, ETH Zurich, Hönggerberg Campus, Wolfgang-Pauli-Str. 10, CH-8093 Zurich, Switzerland

(Received 4 September 2007; accepted 11 October 2007; published online 3 January 2008)

The accurate *first-principles* calculation of relative energies of transition metal complexes and clusters is still one of the great challenges for quantum chemistry. Dense lying electronic states and near degeneracies make accurate predictions difficult, and multireference methods with large active spaces are required. Often density functional theory calculations are employed for feasibility reasons, but their actual accuracy for a given system is usually difficult to assess (also because accurate *ab initio* reference data are lacking). In this work we study the performance of the density matrix renormalization group algorithm for the prediction of relative energies of transition metal complexes and clusters of different spin and molecular structure. In particular, the focus is on the relative energetical order of electronic states of different spin for mononuclear complexes and on the relative energy of different isomers of dinuclear oxo-bridged copper clusters.
 [DOI: 10.1063/1.2805383]

I. INTRODUCTION

The density matrix renormalization group (DMRG) algorithm is a quite new *ab initio* method to solve the many-particle electronic Schrödinger equation as accurately as possible in a full-configuration-interaction (FCI) sense for a given one-electron basis. The DMRG algorithm was developed by White.[1,2] In contrast to other electronic structure methods, DMRG is not based on an expansion of the wave function in terms of Slater determinants, but rather in an adaptive many-particle basis. It also provides a means to systematically approximate the FCI solution as accurately as one desires with only polynomial computational cost, which is a significant advantage over conventional quantum chemical methods. A number of interesting papers showed how DMRG can be applied to quantum chemical Hamiltonians, which shall be briefly reviewed in the following paragraph. For an excellent review ranging from the early beginnings of DMRG in solid state physics to the quantum chemical formulation of DMRG we refer to the work of Schollwöck.[3]

DMRG in quantum chemistry started with the work of Fano *et al.*[4] who performed DMRG calculations on molecular systems using the semiempirical Pariser-Parr-Pople Hamiltonian. Shortly afterwards, White and co-workers[5,6] used the full many-electron Hamiltonian. Several other groups investigated DMRG as well in pioneering studies on benchmark molecules (see Mitrushenkov *et al.*,[7,8] Chan and co-workers,[9–11] and Legeza and co-workers[12–14]). Chan and Head-Gordon provided the first comprehensive description of the DMRG algorithm in quantum chemistry.[15] A fresh look on the algorithm including detailed flow charts was presented in Ref. 16 very recently. The studies of Chan and co-workers comprise benchmark calculations on the dinitrogen ground state potential energy curve,[10] an extension of the DMRG algorithm for nonorthogonal orbitals,[17] a quadratic scaling algorithm,[18] and a harmonic Davidson algorithm.[19] Our group provided a feasibility study on the curve crossing of the two lowest lying electronic states of cesium hydride using relativistically contracted orbitals,[20] systematic studies on the convergence properties of DMRG,[21,22] and recently, a way to decompose DMRG states into a Slater determinant basis,[16] which allows one to understand DMRG convergence in terms of the uptake or rejection of certain electronic configurations for the representation of the DMRG state during the iterations.

The current state of the art DMRG method is still a developmental one, mostly concerned with algorithmic improvements and convergence studies. Nevertheless, it turned out very early in the short history of DMRG that FCI results can be obtained for one-particle active spaces much larger than those usually accessible with standard FCI or complete-active-space self-consistent field (CASSCF) methods. DMRG active spaces can be easily larger than 18 electrons in 18 active spatial orbitals, which may be regarded as the final frontier unsurmountable for CASSCF. This fact in mind, we propose here to apply the DMRG approach to molecules that require huge active spaces already for a *qualitatively* correct description of the wave function.

Regarding well-established standard methods we may note that CASSCF and its restricted-active-space SCF extension—especially, when supplemented by a perturbation theory calculation to capture dynamic correlation contributions that are missing due to the neglect of most virtual orbitals—is a *feasible* and therefore widely applied multireference method to provide qualitatively correct wave functions for open-shell transition metal complexes.[23] The multireference configuration interaction (MRCI) approach appears

[a)]Author to whom correspondence should be addressed. Tel.: ++41-44-63-34308. Fax: ++41-44-63-31594. Electronic mail: markus.reiher@phys.chem.ethz.ch.

to be the only alternative for open-shell systems at the moment. But as any other quantum chemical method, MRCI also has its restrictions such as the need to choose a reference function and to restrict the subsequent orbital substitutions in the wave function to single and double excitations (leaving aside the fact that it is not size consistent, which may be partially cured by a Davidson correction for a small number of electrons). More accurate (multireference) coupled cluster approaches are desirable as they incorporate contributions from the virtual orbitals in the most efficient way, but these are quickly unfeasible for large complexes and clusters. Surely, standard single-reference coupled cluster methods are very valuable for validation purposes of typical *closed-shell* molecules such as ferrocene,[24–26] but the most exciting chemistry takes place at open-shell systems occurring as reactants or intermediates in transition-metal-mediated reactions and catalysis. For these species, CASSCF-type methods are an optimum choice especially if the neglect of many virtual orbitals in the ansatz of the CI-type wave function (the so-called neglect of dynamic correlation effects) is captured afterwards via second-order perturbation theory (PT2) denoted as CASPT2. However, if the CASSCF reference wave function does not adequately represent the electronic structure, which is the case if the CAS cannot be as large as the qualitative picture of the electronic structure would demand, the perturbation correction fails. We will later discuss an example of this type identified by Cramer *et al.*[27,28]

Consequently, the capabilities of DMRG to handle much larger active spaces than CASSCF should be exploited to produce qualitatively correct electronic wave functions and energies. While CASSCF is rather accurate for mononuclear transition metal complexes, this is not necessarily the case if the complexity doubles because the number of transition metal atoms is doubled. Hence, a dinuclear cluster will require at least a twice as large active space. Since the metal atoms in such clusters are often bridged by chalcogen atoms and therefore in close contact, the valence shell orbitals dominated by the atomic orbitals of these bridging atoms need also be included. Thus, transition metal clusters require rather large active spaces and DMRG is capable of handling these.

Therefore, we study DMRG as a potential CASSCF substitute for transition metal *cluster* chemistry in this work. As most challenging test clusters we select the dinuclear oxo-bridged copper clusters identified in Ref. 27 as very difficult cases. But before we can tackle these we are advised to investigate the DMRG algorithm for mononuclear complexes first. The reason for this procedure is the fact that DMRG may easily converge to energies which are higher than the desired FCI energy.[22] This technical problem needs to be overcome in order to assure the accuracy of the results obtained and we therefore consider single-metal molecules first. Because of the well known spin-state-energy problem for mononuclear transition metal complexes,[29–41] we let these first exploratory steps be driven by the desire to calculate the energy of states of different spin reliably.

This work is organized as follows. In Sec. II, we briefly review the DMRG algorithm and apply it in Sec. III first to two mononuclear transition metal complexes carrying only a single ligand. For this purpose we selected CoH and NiCO. Section IV then proceeds to the main target, which are the above-mentioned dinuclear copper clusters. This paper closes with some generally valid conclusions in Sec. V.

II. BRIEF OVERVIEW OF THE DMRG ALGORITHM

Since the DMRG algorithm is not yet widely known and only two detailed formulations with explicit reference to the quantum chemical many-electron Hamiltonian have been published,[15,16] we briefly recall its basic ingredients that are also needed to introduce the notation required in the subsequent sections.

In most of the quantum chemical DMRG publications mentioned in the Introduction, one usually faces the notation that originated from the solid state physics background of DMRG. There, *sites* are occupied by spins on a *lattice* which leads to a direct spatial interpretation of the latter. The whole set of sites is subdivided into three parts of which two are called *system* and *environment*. In the quantum chemical context, however, this picture of having localized sites may be misleading since the orbitals we place on a lattice are spatially delocalized and do not refer to a single point in space. Instead, the actual meaning of having a lattice is to have a certain ordering of the orbitals. To highlight this fact, we stick to the notation of Ref. 16, where system was called *active subsystem* (AS), environment was called *complementary subsystem* (CS), and site was called *orbital* in order to emphasize the abstract nature of the algorithm free of any reference to some physical objects in real space.

The aligned orbitals are divided into three subsystems, two large ones that represent AS and CS, and a block of an (in principle) arbitrary number of single orbitals, which may be called *exactly represented subsystem* (ERS). A subsystem is simply a set of spatial orbitals which are neighbors in the chain of orbitals. The ERS usually consists of two spatial orbitals for feasibility reasons and is located between AS and CS. Each of the three subsystems allows us to construct a many-particle space which is spanned by the orbitals of the subsystem. The many-particle space for a subsystem is a subspace of the Fock space. Matrix representations of operators can be explicitly calculated for the small ERS. It represents $4^2=16$ states if it consists of two spatial orbitals. The spaces of the AS and CS, though, are spanned by m many-particle basis states, with m being a parameter of the DMRG calculation (see below).

For the very first DMRG microiteration step, the size of the AS is chosen such that one can explicitly create all operators needed for the buildup of the *total* electronic Hamiltonian in second quantization,

$$H=\sum_{\substack{i,j\\ \sigma}} h_{ij}a_{i\sigma}^{\dagger}a_{j\sigma}+\frac{1}{2}\sum_{\substack{i,j,k,l\\ \sigma,\sigma'}} V_{ijkl}a_{i\sigma}^{\dagger}a_{j\sigma'}^{\dagger}a_{k\sigma'}a_{l\sigma}, \tag{1}$$

which contains one-electron integrals h_{ij} over orbitals $\phi_i(\mathbf{x})$,

$$h_{ij} = \int \phi_i^*(\mathbf{x}) \left(-\frac{1}{2}\nabla^2 - \sum_I \frac{Z_I}{r_I} \right) \phi_j(\mathbf{x}) d^3x, \tag{2}$$

with the nuclear charge numbers Z_I of the atomic nuclei I and their distances to the electrons $r_I = |\mathbf{r} - \mathbf{R_I}|$ (note that the nucleus-nucleus repulsion term is suppressed for the sake of brevity). The two-electron integrals V_{ijkl} are defined as

$$V_{ijkl} = \int \int \frac{\phi_i^*(\mathbf{x}_1)\phi_j^*(\mathbf{x}_2)\phi_k(\mathbf{x}_2)\phi_l(\mathbf{x}_1)}{r_{12}} d^3x_1 d^3x_2. \tag{3}$$

In general, a DMRG *microiteration* can be divided into three steps.

(*i*) *Solving for the wave function*. The wave function is represented in the (tensor) product space of AS, CS, and ERS. It is of dimension $16m^2$ since AS and CS both contain m basis states and the ERS contains 16 basis states. The product space is restricted to the correct number of particles and projected spin. To determine the ground state wave function Ψ_0, we calculate the matrix representation of the Hamiltonian H_{total}, which is spanned in the basis $\{\text{AS}\} \otimes \{\text{ERS}\} \otimes \{\text{CS}\}$. Since we are usually only interested in the lowest eigenvalue and the corresponding eigenvector of the Hamiltonian, we apply the Davidson iterative subspace procedure[42] to obtain a CI-like representation for the ground state Ψ_0 with expansion coefficients ψ_{IJ}.

(*ii*) *Blocking*. In this step, the AS is enlarged by that orbital of the ERS which follows the AS on the orbital chain. The dimension of the spaces of AS and the single orbital are m and 4, respectively, which means that $4m$ many-particle states are defined on the enlarged subsystem AS′ then. The basis of the enlarged block can be obtained by building the tensor product between the Fock spaces of the active subsystem $\{\text{AS}\}$ and of the single orbital $\{E_{\text{AS}}\}$,

$$\{\text{AS}'\} = \{\text{AS} \times E_{\text{AS}}\} = \{\text{AS}\} \otimes \{E_{\text{AS}}\}. \tag{4}$$

We can now construct the representations of the operators on the enlarged subsystem AS′ by direct multiplication of the corresponding operators from AS and E_{AS}. The dimensions of the operators defined on AS′ are then reduced in a decimation step.

(*iii*) *Decimation*. The enlarged subsystem AS′ of dimension $4m$ is transformed to a new many-particle basis of dimension m. The decimated system block is then used as a starting point for the next microiteration. The density matrix $D_{\text{AS}'}$ of the enlarged active subsystem AS′ can be calculated from the ground state wave function Ψ_0 expressed by the CI-type expansion coefficients ψ_{IJ} according to

$$D_{II'} = \sum_J \psi_{IJ}\psi_{I'J}^* \overset{\psi_{IJ}\ \text{real}}{=} \sum_J \psi_{IJ}\psi_{I'J}. \tag{5}$$

This evaluation is possible because we know from the construction of the Hamiltonian matrix that an eigenvector Ψ of the Hamiltonian can be written as a tensor product of many-particle states χ_I of the enlarged active subsystem AS′ and of many-particle states χ_J of the complementary subsystem CS plus the remaining exactly represented orbitals,

$$|\Psi\rangle = \sum_{IJ} \psi_{IJ}\chi_I \otimes \chi_J. \tag{6}$$

The reduced density matrix is then diagonalized,

$$D_{\text{AS}'} = \sum_i w_i |A_i\rangle\langle A_i|. \tag{7}$$

The eigenvalues w_i of the reduced density matrix can be interpreted as the weights of the eigenstates. We now have a sophisticated way of choosing an $(m \times 4m)$-dimensional rectangular renormalization matrix C built from the eigenvectors $|A_i\rangle$ of the reduced density matrix with highest weights w_i.

The transformation to the truncated basis is called *renormalization*. The old operators O^{old} of AS′ are renormalized to lower dimensional new operators O^{new},

$$O^{\text{new}} = C^T O^{\text{old}} C, \tag{8}$$

where C is the renormalization matrix built up from m eigenvectors of $D_{\text{AS}'}$. If the $m \times 4m$ matrix C were square, Eq. (8) would be a unitary transformation. Since C is not a square matrix, the transformation eliminates those states which are less important if the optimum representation of reduced dimension is sought for in a least-squares sense.

A sequence of DMRG microiteration steps from left to right along the orbital chain is called a *sweep*. If the sweep reaches the end of the orbital chain, the sweep terminates and the direction is reversed. The next sweep commences now in the reversed direction along the chain of orbitals.

III. PERFORMANCE OF DMRG ON THE SPIN STATE PROBLEM

After having discussed the basics of the DMRG algorithm, we now apply it to states of different spin for two prototypical transition metal complexes carrying only a single ligand. We choose CoH and NiCO as examples. The latter molecule is electronically more complex due to the CO ligand (capable of accepting back-donation from the metal atom in the Dewar-Chatt-Duncanson picture[43,44]) when compared to the simple σ-donor ligand H in CoH.

A. CoH

Our primary goal is to investigate the applicability of the DMRG algorithm to determine the difference between the calculated singlet and triplet energies, which is difficult to calculate with any quantum chemical method (see the references given in the Introduction). Cobalt hydride is a small molecule particularly suited for the assessment of the reliability of the DMRG algorithm. We focus on the DMRG calculation of the triplet ground state and the energetically lowest lying state of singlet symmetry with various numbers of DMRG renormalized system states m and compare the converged energy with the CASSCF reference energy. The different choices for m are needed in order to identify a potential convergence of a single run to a local energy minimum. In this way we avoid to interpret single sets of total energies for both spin states of which one or even both energies did not converge to the complete-active space CI (CAS-CI) energy, which is the exact reference for the DMRG calculation.

TABLE I. First set: CAS(10,14) in C_{2v} symmetry of the CoH molecule. The doubly occupied orbitals in the reference determinant are marked in bold face type and singly occupied are underlined. Second set: CAS(10,10) in C_{2v} symmetry of the CoH molecule. The doubly occupied orbitals in the reference determinant are marked in bold face type and singly occupied are underlined. The sequence of orbitals represents the orbital ordering employed in the DMRG calculations.

Spin state	Active orbitals							
	CAS(10,14)							
Singlet	$\mathbf{6a_1}$	$\mathbf{7a_1}$	$\mathbf{8a_1}$	$9a_1$	$10a_1$	$11a_1$	$12a_1$	$\mathbf{3b_1}$
	$4b_1$	$5b_1$	$3b_2$	$4b_2$	$5b_2$	$\mathbf{1a_2}$		
Triplet	$\mathbf{6a_1}$	$\underline{7a_1}$	$\underline{8a_1}$	$9a_1$	$10a_1$	$11a_1$	$12a_1$	$\mathbf{3b_1}$
	$4b_1$	$5b_1$	$\mathbf{3b_2}$	$4b_2$	$5b_2$	$\mathbf{1a_2}$		
	CAS(10,10)							
Singlet	$\mathbf{6a_1}$	$\mathbf{7a_1}$	$\mathbf{8a_1}$	$9a_1$	$10a_1$	$\mathbf{3b_1}$	$4b_1$	$3b_2$
	$4b_2$	$\mathbf{1a_2}$						
Triplet	$\mathbf{6a_1}$	$\underline{7a_1}$	$\underline{8a_1}$	$9a_1$	$10a_1$	$\mathbf{3b_1}$	$4b_1$	$\mathbf{3b_2}$
	$4b_2$	$\mathbf{1a_2}$						

All preparatory calculations described in this and in the following sections, which produce the one-electron and two-electron integrals, h_{ij} and V_{ijkl}, respectively, as well as the CASSCF, CASPT2, and density functional theory (DFT) reference results, were carried out with the MOLPRO program package.[45] All DMRG calculations were performed with the DMRG programs developed in our group. We study the two spin states of the cobalt hydride molecule at a bond distance of 156.271 pm, which was obtained by a structure optimization using CCSD(T) and a Dunning cc-pVTZ basis set.[46,47] The final Hartree-Fock occupation in C_{2v} symmetry for the singlet state is $1a_1^2-8a_1^2$, $1b_1^2-3b_1^2$, $1b_2^2-2b_2^2$, and $1a_2^2$; and $1a_1^2-6a_1^27a_1^18a_1^1$, $1b_1^2-3b_1^2$,$1b_2^2-3b_2^2$, and $1a_2^2$ for the triplet state.

For the CASSCF calculation, we employ two active spaces consisting of 10 and 14 molecular orbitals, respectively, occupied by ten electrons each. The molecular orbitals are chosen according to the occupation and orbital coefficients of the Hartree-Fock orbitals and are listed in Table I. The CASSCF(10,10) and the CASSCF(10,14) results are then used as a reference for the DMRG calculations and are given in Table II.

For the subsequent DMRG calculations the initial occupation was determined according to the Hartree-Fock configuration. We consider 10 and 14 natural orbitals, i.e., the same active spaces as in the CASSCF reference calculations, and a sequence of 32, 60, 64, 100, 200, 400, and 600 renormalized states m. Up to 400 microiterations were required until convergence of the energy was achieved. For the singlet calculation, a level shift performed on the many-electron Hamiltonian H,

$$H_{\text{shift}} = H + \alpha S_- S_+ = H + \alpha(S^2 - S_z^2 - S_z), \tag{9}$$

was applied in order to obtain a wave function of pure spin. This prevents the occurrence of states which possess the same projected spin (i.e., the same M_S eigenvalue of S_z) but a different total spin S. The unwanted spin states with a higher multiplicity are affected by the level shift operator and augmented by an energy shift proportional to the parameter α. Tests showed that a value of $\alpha=1$ is sufficient in most cases. Energies presented in this work have been obtained by diagonalization of the shifted Hamiltonian H_{shift}. The one-electron and two-electron integrals were calculated from CASSCF orbitals based on the same active space presented in Table I. In Table II the vertical energy splitting of the singlet and triplet states of cobalt hydride is listed for the CASSCF and CASPT2 reference as well as for the DMRG calculations with an increasing number of m renormalized DMRG system states.

TABLE II. Results of CASSCF and CASPT2 reference and DMRG calculations for the singlet and triplet states of CoH for ten electrons distributed over ten active spatial orbitals in hartree atomic units. Relative energies are given in kJ mol^{-1}. The first set of DMRG calculations employed a CAS of ten orbitals, while the latter the one consisting of 14 orbitals. It is interesting to note the deviating DMRG calculation marked by the superscript a. Here, during the first 150 microiterations 32 DMRG basis states were used and afterwards changed to 60 DMRG basis states for the next 250 microiterations.

Method	$E_{\text{singlet}}(E_h)$	$E_{\text{triplet}}(E_h)$	ΔE(kJ mol^{-1})
DMRG(m=32)	−1381.942 837 45	−1381.994 947 72	136.8
DMRG(m=60)	−1381.943 854 89	−1381.995 091 39	134.5
DMRG(m=64)	−1381.952 033 91	−1381.995 096 08	113.1
DMRG(m=100)	−1381.952 064 07	−1381.995 107 66	113.0
DMRG(m=200)	−1381.952 073 84	−1381.995 110 42	113.0
DMRG(m=400)	−1381.952 073 95	−1381.995 110 45	113.0
DMRG(m=600)	−1381.952 073 95	−1381.995 110 45	113.0
CASSCF(10,10)	−1381.952 073 95	−1381.995 110 45	113.0
CASPT2(10,10)	−1382.189 526 76	−1382.241 333 74	136.0
DMRG(m=32)	−1381.964 667 68	−1382.017 236 98	138.0
DMRG(m=60)	−1381.959 381 80	−1382.020 096 40	159.4
DMRG(m=60^a)	−1381.972 877 48	−1382.020 096 40	124.0
DMRG(m=64)	−1381.977 619 31	−1382.020 167 82	111.7
DMRG(m=100)	−1381.979 696 65	−1382.020 506 76	107.2
DMRG(m=200)	−1381.977 099 88	−1382.020 751 52	114.6
DMRG(m=400)	−1381.981 062 29	−1382.020 808 17	104.4
DMRG(m=600)	−1381.981 090 47	−1382.020 812 76	104.3
CASSCF(10,14)	−1381.981 097 35	−1382.020 813 74	104.3
CASPT2(10,14)	−1382.192 370 84	−1382.242 103 09	130.6
DFT/BP86	−1383.504 018 73	−1383.585 211 82	213.1
DFT/B3LYP*	−1383.031 402 31	−1383.106 305 78	196.7
DFT/B3LYP	−1383.202 267 27	−1383.279 574 17	203.0

From the reference calculation we know that more configurations are needed to properly describe the singlet state compared to the number of configurations for the triplet state. In the DMRG algorithm, we apply for each calculation a fixed number of renormalized states m. We may therefore assume that the triplet state is better described than the singlet in a DMRG calculation. Still, the energy difference is already converged to 0.1 kJ mol^{-1} in the case of the large CAS by selecting only m=400 renormalized states.

The DMRG calculations employing the large CAS produced two outliers for the singlet state with m=60 and m=200, which turned out to be too high in energy. The outlier for m=60 could be corrected by reducing the number of DMRG states to 32 for 150 microiterations and then switch-

ing back to the desired 60 DMRG states. This procedure, described in Ref. 22, allowed us to capture all important configurations which were not picked up in the standard setup (see Ref. 16 for a detailed investigation of such cases). Despite the occurrence of these outliers, the overall picture is very satisfactory in the sense that by increasing the number of DMRG states the spin splitting converges. The effect of the enlarged CAS(10,14) compared to the CAS(10,10) on the DMRG calculation manifests in a slower convergence of the energy splitting between the singlet and triplet states. We also notice that the absolute energy values for the CASSCF(10,14) calculations of the singlet and triplet states are deviating by about 0.03 a.u. from the energy values of the CASSCF(10,10) calculations, whereas the difference in the absolute energies of the CASPT2(10,14) and CASPT2(10,10) calculations is of the order of 0.003 a.u. The CASPT2 results are—irrespective of the CAS chosen—20–30 kJ mol^{-1} lower in energy than our best DMRG results with 600 DMRG states m, which indicates the magnitude of dynamic correlation effects neglected in a standard DMRG calculation. The DFT/BP86,[48,49] DFT/B3LYP*,[32] and DFT/B3LYP (Refs. 50 and 51) calculations yield similar energy splittings around 200 kJ mol^{-1}, which are strongly deviating from all our DMRG, CASSCF, and CASPT2 results. Because of the multireference character of the wave function of CoH with two near-degenerate electronic singlet states often poorly described by DFT and considering the fact that CASPT2 incorporates dynamical electron correlation through a perturbative inclusion of the virtual orbitals (the CASPT2 energy values are also only slightly changing by increasing the active space), we may assume that the pure and hybrid DFT calculations provide a qualitatively wrong description of the energy splitting between the singlet and triplet states of CoH.

The critical DMRG(10,14) singlet calculation for $m=60$ in Table II demonstrates that the DMRG algorithm may converge to a stationary point (being a local minimum or a saddle point). For such cases, Chan and co-workers[15,19] recommend to add random noise to the density matrix in order to force the mixing of configurations that would have not been captured otherwise if m is chosen to be too small. If we add small numbers 10^{-n}, with $n=8$, 9, 10, 11, and 12, to all entries of each block of the density matrix, where each block corresponds to states of the same particle number and projected spin, we note that the energy drops down to −1381.960 005, −1381.972 565, −1381.972 580, −1381.973 611, and −1381.973 531 hartree, respectively. Thus, the addition of some noise may improve the absolute energy in cases where the seemingly converged energy is too high. In the case of the second critical singlet calculation with $m=200$, however, the addition of noise to the density matrix improves the energy only insignificantly up to −1381.977 201 hartree, which is still considerably higher than the −1381.979 697 hartree obtained from the calculation with the smaller value $m=100$. On the other hand, the sequence of energies for different m values allows us to obtain a very good estimate for the relative energy independent of a single result from a single calculation with a given value of m. We should also note that we got similar results for the Cr_2 example studied in Ref. 22, where the total energy got stuck in one case at −2086.1379 hartree, while the best calculation with an optimized ordering of the orbitals on the chain yielded −2086.3379 hartree. Adding noise with $n=6$, 9, and 11 yields in this case −2086.1058, −2086.1899, and −2086.1369 hartree. Thus, also in the Cr_2 case the energy may improve but does not approach the reference value.

TABLE III. Active orbitals for the singlet and triplet CASSCF and DMRG calculations of NiCO in C_s symmetry. Doubly occupied orbitals in the Hartree-Fock reference determinant are marked in bold face. In the case of the triplet state orbitals $16a_1$ and $17a_1$ are singly occupied. The second sequence of orbitals also represents the orbital ordering employed in the DMRG calculations.

CASSCF	**$11a_1$**	**$12a_1$**	**$13a_1$**	**$14a_1$**	**$15a_1$**	**$16a_1$**	$17a_1$	$18a_1$	$19a_1$	$20a_1$
	$21a_1$	**$3a_2$**	**$4a_2$**	**$5a_2$**	$6a_2$	$7a_2$				
DMRG	**$7a_1$**	**$8a_1$**	**$9a_1$**	**$10a_1$**	**$11a_1$**	**$12a_1$**	**$13a_1$**	**$14a_1$**	**$15a_1$**	**$16a_1$**
	$17a_1$	$18a_1$	$19a_1$	$20a_1$	$21a_1$	$22a_1$	$23a_1$	$24a_1$	$25a_1$	$26a_1$
	$27a_1$	$28a_1$	$29a_1$	$30a_1$	$31a_1$	$32a_1$	$33a_1$	**$2a_2$**	**$3a_2$**	**$4a_2$**
	$5a_2$	$6a_2$	$7a_2$	$8a_2$	$9a_2$	$10a_2$	$11a_2$	$12a_2$	$13a_2$	

It is evident that at the level of 600 DMRG states the DMRG algorithm reproduces the CASSCF energy of the cobalt hydride within the same active space. We demonstrated that DMRG calculations for 200, 400, and 600 renormalized states can produce a consistent picture on DMRG convergence and provide an accurate relative energy of the two spin states. This indicates that the DMRG algorithm is suitable for calculations of the spin state splitting in transition metal complexes. We may now investigate the second, more complex example, namely, NiCO.

B. NiCO

This section presents DMRG calculations on the singlet and triplet spin states of the NiCO molecule, which can be considered as a prototypical carbonyl metal complex. All preparatory calculations of the one- and two-electron integrals in the molecular orbital basis as well as all DFT and CASSCF calculations have been performed using the MOLPRO package of *ab initio* programs.[45] The bond distances were set to 168.389 pm for NiC and 114.893 pm for CO, which were obtained by structure optimization with DFT/B3LYP (Refs. 50 and 51) and a Dunning cc-pVTZ basis set.[46,47] These structural parameters are in very good agreement with the data collected and reported for various quantum chemical methods in Ref. 52. For the reference CASSCF calculations we have employed 18 electrons in 16 active orbitals for the singlet and triplet states. The active spaces for the CASSCF and for the DMRG calculations are given in Table III.

The 39 natural orbitals needed for the DMRG calculations were produced with the help of smaller CASSCF calculations, where we have used 10 active orbitals for the singlet state and 11 active orbitals for the triplet states. Afterwards, all orbitals were transformed to natural orbitals and a DMRG active space of 39 natural orbitals was selected. The one-electron and two-electron integrals, h_{ij} and V_{ijkl}, respectively, were calculated in the basis of the 39 natural CASSCF orbitals.

TABLE IV. Performance of DMRG in comparison to CASSCF and DFT for lowest lying singlet and triplet spin states of the NiCO molecule employing a cc-pVTZ basis set and 16 active natural orbitals from the CASSCF calculations. The DMRG vertical excitation energies were obtained for the same setup but with 39 active natural orbitals in the DMRG calculations. Coupled cluster results have been taken from Ref. 52. Note that Ref. 52 only provides the total energy of the triplet state for an adiabatic excitation. The adiabatic excitation energies are −50.9 kJ mol^{-1} for CCSD/ANO-TZ and −115.2 kJ mol^{-1} for CCSD(T)/ANO-TZ.

Method	$E_{\text{singlet}}(E_h)$	$E_{\text{triplet}}(E_h)$	ΔE(kJ mol^{-1})
DMRG(m=200)	−1619.871 519	−1619.845 027	−69.6
DMRG(m=400)	−1619.881 770	−1619.854 491	−71.6
DMRG(m=600)	−1619.886 757	−1619.859 160	−72.5
DMRG(m=800)	−1619.889 232	−1619.861 482	−72.9
DMRG(m=1200)	−1619.891 536	−1619.863 724	−73.0
CASSCF(18,16)	−1619.856 677	−1619.819 003	−98.9
DFT/BP86	−1622.022 509	−1621.951 771	−185.7
DFT/B3LYP*	−1621.377 705	−1621.321 455	−147.7
DFT/B3LYP	−1621.608 140	−1621.557 320	−133.4
CSD/ANO-TZ[a]	−1620.402 54		−95.5
CCSD(T)/ANO-TZ[a]	−1620.475 16		−151.5

[a]Reference 52.

We have considered 200–1200 renormalized states m per active subsystem. Each calculation is converged with respect to the number of microiteration steps. For the singlet calculation, a level shift was applied according to Eq. (9) in order to obtain pure spin states. In Table IV, the DMRG calculated energies are shown in comparison to CASSCF and CCSD(T) results.

The DMRG energy difference of the singlet and triplet states is monotonically converging with the number of states m. Already for m=200 states, the *relative* energies are essentially converged, especially in view of the general spread of such results obtained with other quantum chemical methods as highlighted by the data given in Table IV. The total energies, however, are not fully converged and even change in the largest DMRG calculations from m=800 to m=1200. This is an important result as it demonstrates that one may obtain reliable relative energies from DMRG calculations even if the total energy is not fully converged with respect to the number of renormalized system states m. Of course, also the relative energy is not fully converged, but its changes are below 1 kJ mol^{-1}—as our calculations show—and are thus below the accuracy needed for chemical purposes.

The restriction of DMRG to a small number of m basis states is, in principle, comparable to the restriction to certain excitations in CI and CC models that lead to the CISD, CISDT,…, and CCSD, CCSDT,…, models, respectively. But in the case of DMRG, the restriction of the basis defined by the size of m always features the DMRG optimization condition, namely, that the reduced-dimensional space in which the total wave function is represented obeys a least-squares-fit condition by virtue of the renormalization procedure. The comparatively small number of m basis states must not be confused with electronic configurations as each of these DMRG basis states represents a FCI-type expansion into all electronic configurations constructable within the active space chosen.[16] Hence, one may obtain reliable relative DMRG energies with comparatively moderate computational cost since the total electronic energy does not need to be fully converged with respect to m.

Compared to the CASSCF results, the total DMRG energies for both the singlet and triplet states is much lower, which is due to the larger active space. Single-reference CCSD coupled-cluster calculations carried out by Horný *et al.*[52] yield a vertical energy difference of −95.5 kJ mol^{-1} comparable to the CASSCF energy difference of −98.9 kJ mol^{-1}. The DMRG data, however, show that the complete active space in the CASSCF calculation was not as large as it should be since the DMRG vertical excitation energy converges to −73.0 kJ mol^{-1}. Then, inclusion of the perturbatively treated triples excitations in CCSD(T) (Ref. 52) increases the absolute value of the CCSD energy gap and yields −151.5 kJ mol^{-1}. But as already mentioned above, the relative vertical energies obtained with all methods differ very much and the accuracy of the single-reference CCSD(T) for this multireference case is not clear. Unfortunately, there are no experimental results available for the vertical excitation energy from the singlet to the triplet state. In any case, the DMRG result may be considered as a converged CAS-CI result, which is lacking contributions from dynamic correlation effects.

Although we have considered two small transition metal molecules so far, DMRG is, of course, also able to treat larger complexes because the computer time determining ingredient is the number of active orbitals rather than the number of atomic nuclei in the molecule. Hence, molecular orbitals located mainly on spectator ligands can easily be kept frozen in a DMRG calculation. We will encounter such larger molecules in the next section.

IV. RELATIVE ENERGIES OF DINUCLEAR COPPER CLUSTERS

After having demonstrated the capabilities of DMRG for the spin state problem in transition metal chemistry, we now consider the question of a reliable calculation of relative energies on a given potential energy hypersurface of the same total spin. Since DMRG is ideally suited for the calculation of electronic structures that require huge active spaces even for a qualitatively correct description of the ground state wave function, we choose transition metal clusters with two copper atoms and two bridging oxygen atoms. As mentioned in the Introduction such dicopper clusters have been recently investigated by Cramer *et al.*[27,28] and were found to be challenging systems for all electronic structure methods.

We should also note that these dicopper complexes and their reliable quantum chemical treatment are of tremendous importance in coordination and bioinorganic chemistry–which was the starting point for the work of Cramer *et al.*[27,28] Activation of dioxygen is mediated by copper-containing metalloproteins such as oxyhemocyanin and oxytyrosinase.[53,54] There exist several reviews on dicopper-oxygen complexes[55–57] which play an important role as catalysts and in active centers of enzymes. Usually, such dinuclear complexes are studied within the framework of broken-symmetry DFT. But in view of the fact that the approximate nature of present-day density functionals prohibits

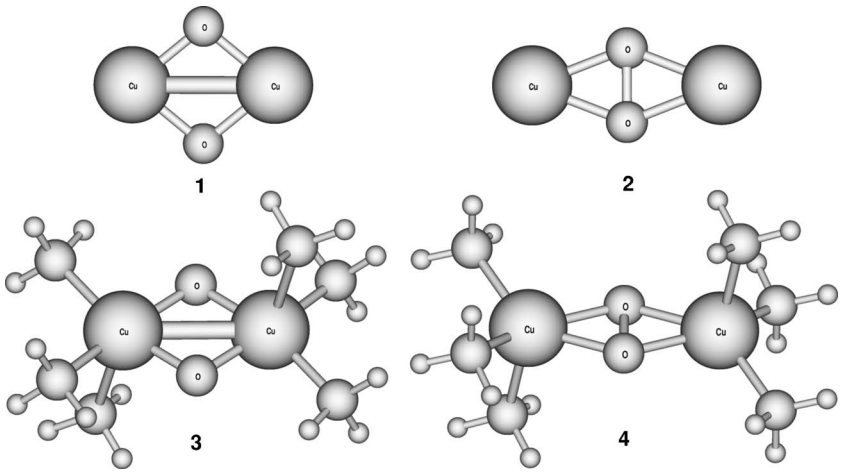

FIG. 1. Structures of the $[Cu_2O_2]^{2+}$ isomers $[Cu_2(\mu\text{-}O)_2]^{2+}$ **1** and $[Cu_2(\mu\text{-}\eta^2\text{:}\eta^2\text{-}O_2)]^{2+}$ **2** and of the $\{[(NH_3)_3Cu]_2O_2\}^{2+}$ isomers $\{[(NH_3)_3Cu]_2(\mu\text{-}O)_2\}^{2+}$ **3** and $\{[(NH_3)_3Cu]_2(\mu\text{-}\eta^2\text{:}\eta^2\text{-}O_2)\}^{2+}$ **4**.

a systematic improvement of the results obtained, broken-symmetry studies are affected by a high degree of uncertainty when it comes to the assessment of the reliability of the results. Also, accurate *ab initio* reference data are lacking and DMRG may provide a way out of this dilemma.

Two main motifs of metal-containing cores containing two copper ions were synthetically characterized, the bis(μ-oxo) $[Cu_2(\mu\text{-}O)_2]^{2+}$ (**1**) and the peroxo $[Cu_2(\mu\text{-}\eta^2\text{:}\eta^2\text{-}O_2)]^{2+}$ (**2**) cores.[58] Cramer *et al.*[59] examined the interconversion of the model compounds $\{[(NH_3)_3Cu]_2(\mu\text{-}O)_2\}^{2+}$ (**3**) and $\{[(NH_3)_3Cu]_2(\mu\text{-}\eta^2\text{:}\eta^2\text{-}O_2)\}^{2+}$ (**4**) using multireference second-order perturbation theory (CASPT2) with eight electrons in eight orbitals active space. They found that the $\mu\text{-}\eta^2\text{:}\eta^2$ peroxo form is slightly favored by electrostatic interactions but both isomers are almost equal in energy and that the energetical barrier for their interconversion is small. This was also experimentally concluded by Tolman.[60] Due to the flat potential energy surface along the interconversion, the ability of the dicopper-dioxygen isomers to rapidly equilibrate was obvious and documented by Mahapatra *et al.*[61] In Fig. 1 the structures of the four clusters **1**–**4** are depicted.

The interconversion pathway between the $\mu\text{-}\eta^2\text{:}\eta^2$ peroxo and bis(μ-oxo) isomers, where each copper ion is equipped with three NH_3 ligands, was discussed in a study by Flock and Pierloot.[62] After comparing the performance of DFT/B3LYP and CASPT2 on the two isomers, they reported that broken-symmetry DFT calculations are not able to capture the most important correlation effects in the bis(μ-oxo) structure and that CASPT2 reveals an intrinsic stabilization of the $\{[(NH_3)_3Cu]_2(\mu\text{-}O)_2\}^{2+}$ compound. The huge difference between the results of the two isomers obtained by DFT/B3LYP and CASPT2 was due to varying nondynamical and dynamical correlation effects along the isomerization pathway. Based on their findings, they concluded that the presence of the $\{[(NH_3)_3Cu]_2(\mu\text{-}\eta^2\text{:}\eta^2\text{-}O_2)\}^{2+}$ structure in respiratory proteins must be traced back to the presence of bulky capping ligands or to electrostatic solvent effects. In the work of Rode and Werner[63] the two isomers were reinvestigated using a localized orbital description and multireference configuration interaction with a Davidson correction (MRCI+Q) method.[63] It was claimed that CASPT2 strongly overestimates the correlation effects. MRCI+Q predicts the $\mu\text{-}\eta^2\text{:}\eta^2$ peroxo structure to be favored, which is in qualitative agreement with DFT/B3LYP and x-ray experiment for hemocyanine.[64,65] On the other hand, DFT/B3LYP seems to stabilize the biradical $\mu\text{-}\eta^2\text{:}\eta^2$ peroxo isomer too much. This effect depends approximately linearly on the amount of exact exchange in the density functional. A couple of years ago, we proposed to scale the amount of exact exchange in the exchange density functional down to at least 15%,[32–34] which became known as the B3LYP* functional. Indeed, the DFT/B3LYP* calculations in Ref. 63 turned out to be in good agreement with the MRCI+Q results. Then, Cramer *et al.*[27,28] performed another study on the isomerization pathway of the $\mu\text{-}\eta^2\text{:}\eta^2$ peroxo and bis(μ-oxo) dicopper cluster applying a wide variety of theoretical models with special emphasis on the problem of maintaining a balanced description of rapidly changing dynamical and nondynamical electron correlation effects and a varying degree of biradical character. A qualitatively correct description of the relative energies compared to experimental results[55] is achieved by completely renormalized coupled cluster and surprisingly by pure density functional theory. Hybrid density functionals underestimate the stability of the bis(μ-oxo) form by almost a factor of 2. Single-root CASPT2 overestimates the stability of the bis(μ-oxo) form and even gives a qualitatively wrong result (both in comparison to MRCI calculations), as Rode and Werner have already noticed. Selected results of these studies relevant to this work have been collected in Table V.

Our goal is to reinvestigate the relative energies of the $[Cu_2(\mu\text{-}\eta^2\text{:}\eta^2\text{-}O_2)]^{2+}$ and $[Cu_2(\mu\text{-}O)_2]^{2+}$ cores as well as that of the $\{[(NH_3)_3Cu]_2(\mu\text{-}\eta^2\text{:}\eta^2\text{-}O_2)\}^{2+}$ and $\{[(NH_3)_3Cu]_2(\mu\text{-}O)_2\}^{2+}$ clusters and to show that the DMRG algorithm is capable of handling a varying degree of dynamical and nondynamical correlation effects to predict qualitatively correct energies.

A. Qualitative picture of the electronic structure

It is instructive to first study a qualitative picture of the electronic structure of the $Cu_2O_2^{2+}$ isomers in terms of an extended Hückel theory molecular orbital (MO) diagram[66] by the YAeHMOP program.[67] We want to show that the active space of a binuclear transition metal cluster cannot be

TABLE V. Energy differences $\Delta E_{12}=E(\mathbf{1})-E(\mathbf{2})$ and $\Delta E_{34}=E(\mathbf{3})-E(\mathbf{4})$ in kJ mol^{-1} from the work of Cramer *et al.* (Refs. 27 and 28) Rode and Werner (Ref. 63) and Flock and Pierloot (Ref. 62). A detailed description of the orbitals included in the active space of the reference calculations can be found in the corresponding literature. "bs" denotes a broken-symmetry solution.

Method	ΔE_{12}	ΔE_{34}
CASSCF(8,8)[a]	−15.6	74.0
CASSCF(16,14)[a]	1.0	124.7
CASSCF(8,10)[b]		97.1
CASSCF(8,10)[c]		97.9
CASPT2(8,8)[a]	27.2	−50.6
CASPT2(16,14)[a]	6.0	−71.9
CASPT2(8,10)[b]		−48.1
CASPT2(12,14)[b]		−53.1
CASPT2(8,6)[c]		−51.1
CASPT2(8,10)[c]		−42.8
MRCI+Q(8,6)[c]		48.6
CCSD(T)[a]	128.0	26.4
BLYP[a]		35.0
bs-B3LYP[a]	221.3	85.4

[a]Reference 27.
[b]Reference 62.
[c]Reference 63.

handled using the standard CASSCF approach anymore because it cannot cope with all relevant active orbitals. A subsequent CASPT2 calculation thus cannot be expected to cure this defect. Figure 2 demonstrates that the relevant active space for a correct description of the bis(μ-oxo) $[Cu_2O_2]^{2+}$ isomer is doubled with respect to the active space of a mononuclear complex. The MO diagram is produced for two CuO^+ fragments and consists of the valence atomic orbitals (AOs) of Cu and O which sum up to 26 MOs in total (for clarity the MOs originating from the interaction of the oxygen 2*s* orbitals are omitted in Fig. 2).

A detailed analysis of the composition of the molecular orbitals leads to the classification of the 26 MOs into three segments marked by Fig. 2. Box **A** comprises MOs which are predominantly composed of Cu 3*d* and O 2*p* AOs. Box **A** may be subdivided again into three areas where the first one contains six bonding orbitals as linear combinations of Cu 3*d* and O 2*p* AOs. The next four MOs are essentially nonbonding Cu $3d_{xy}$, $3d_{x^2-y^2}$, $3d_{xz}$, and $3d_{z^2}$ AOs. The last six MOs are then the antibonding linear combinations of Cu 3*d* and O 2*p* AOs. The two MOs in box **B** are mainly the Cu 4*s* AOs with small contributions from the Cu $4p_z$ and O $2p_z$ AOs. Box **C** comprises six MOs with Cu 4*p* and O 2*p* characters. The extended Hückel theory calculation is sufficient to demonstrate that in binuclear transition metal clusters the one-particle active space must be doubled compared to the mononuclear analog if one aims at a qualitatively correct description of the electronic structure. In analogy of this argument, the active space of a trinuclear clusters would have to be tripled, which would correspond to about 50 active orbitals in this case.

Note also that Pierloot suggests the inclusion of a second *d* shell in a multireference treatment to obtain accurate results.[68] This corresponds to an increase of the active space of five MOs per transition metal. At present, DMRG is the only method to handle active spaces of such dimension if a CASSCF-type wave function is sought for.

B. DMRG performance for relative energies on the same potential energy surface

All preparatory calculations were again performed with the MOLPRO package.[45] For Cu we employed the same basis set as Cramer *et al.*,[27,28] namely, the Stuttgart pseudopotential and associated basis functions (ECP10MDF).[69] The atomic natural orbital (ANO) basis set of Pierloot *et al.* was used for O.[70] The basis set of Pierloot *et al.*, however, did not feature the $[10s6p3d|4s3p2d]$ contraction scheme for O as reported in Ref. 27. For calculations on **1** and **2** with an active space of 32 orbitals, which corresponds to entries 1 and 2 in Table VII, the ANO basis set of Pierloot *et al.* was used with a $[10s6p3d|7s6p3d]$ contraction (denoted as BS1 in the following). After publication of the reference to the second contraction scheme,[28] subsequent calculations were performed also with this $[14s9p4d|4s3p2d]$ contraction of the ANO basis set[71] and are denoted as BS2 in the following. For CASSCF and CASPT2 calculations on **3** and **4**, we chose the ANO basis set of N with the same contraction scheme as used for O, whereas for H we applied a $[8s4p|2s1p]$ contraction, belonging to BS2 as well. How-

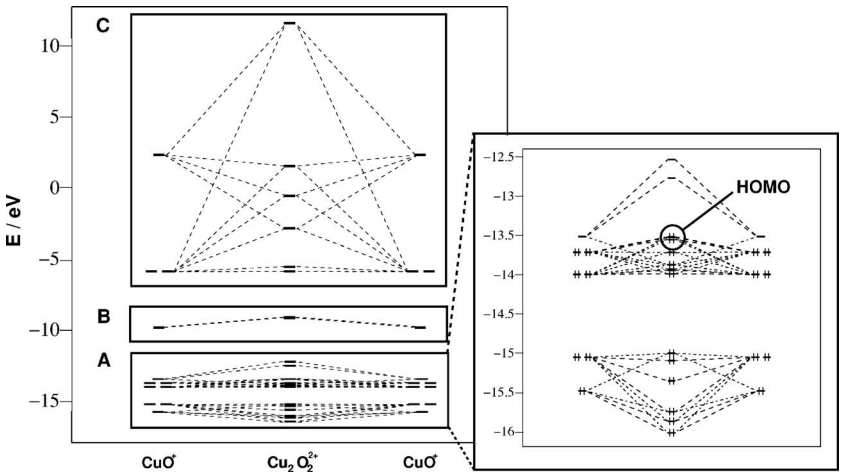

FIG. 2. The molecular orbital diagram as obtained from extended Hückel calculations (Ref. 67). The molecular orbitals for the interaction of the oxygen 2*s* orbitals at −33.47 and −32.27 eV were omitted for clarity in the diagram in the left panel. In the right panel, box **A** is scaled up for a better presentation of the molecular orbitals dominated by the 3*d* orbitals on the copper atoms and 2*p* orbitals of the oxygen atoms. Boxes **B** and **C** contain the molecular orbitals dominated by 4*s*- and 4*p*-type orbitals of the copper centers, respectively. Note that two orbitals in part B are lying on top of each other with energies of −9.182 and −9.137 eV.

TABLE VI. Active spaces for the CASSCF calculation for the μ-η^2:η^2 peroxo and bis(μ-oxo) $[Cu_2O_2]^{2+}$ cores in D_{2h} symmetry (top). Active spaces for the CASSCF calculation for the μ-η^2:η^2 peroxo and bis(μ-oxo) $\{[(NH_3)_3Cu]_2O_2\}^{2+}$ molecules in C_{2v} symmetry (bottom). Doubly occupied orbitals in the Hartree-Fock reference determinant are marked in bold face.

Method	Active space for **1** and **2**							
CAS(8,8)	$\mathbf{7a_g}$	$8a_g$	$\mathbf{4b_{2u}}$	$5b_{2u}$	$\mathbf{5b_{1u}}$	$6b_{1u}$	$\mathbf{2b_{3g}}$	$3b_{3g}$
CAS(16,14)	$\mathbf{5a_g}$	$\mathbf{6a_g}$	$\mathbf{7a_g}$	$8a_g$	$\mathbf{4b_{2u}}$	$5b_{2u}$	$6b_{2u}$	$\mathbf{3b_{1u}}$
	$\mathbf{4b_{1u}}$	$\mathbf{5b_{1u}}$	$6b_{1u}$	$\mathbf{2b_{3g}}$	$3b_{3g}$	$4b_{3g}$		
Method	Active space for **3** and **4**							
CAS(8,8)	$\mathbf{18a_g}$	$19a_g$	$\mathbf{11a_u}$	$12a_u$	$\mathbf{17b_u}$	$18b_u$	$\mathbf{10b_g}$	$11b_g$
CAS(16,14)	$\mathbf{17a_g}$	$\mathbf{18a_g}$	$19a_g$	$\mathbf{10a_u}$	$\mathbf{11a_u}$	$12a_u$	$13a_u$	$\mathbf{16b_u}$
	$\mathbf{17b_u}$	$18b_u$	$\mathbf{9b_g}$	$\mathbf{10b_g}$	$11b_g$	$12b_g$		

ever, for the calculation of the one- and two-electron integrals needed for the DMRG calculations on clusters **3** and **4**, the basis sets for N and H were reduced for feasibility reasons to a DZP and DZ basis sets,[72] respectively, which yield a basis set designated as BS3 in the following.

To all CASPT2 calculations a level shift of 0.1 a.u. was applied. In our cases, intruder states did not appear to pose any significant problems. CASSCF canonical orbitals have been used to speed up the CASPT2 calculations. All optimized geometries have been taken from the supporting information of Refs. 27 and 28. These structures were optimized by Cramer and co-workers using the B3LYP density functional.

Active spaces are defined in Tables VI and VII for the CAS(16,14) and CAS(8,8) calculations as well as for the calculation of the one- and two-electron integrals. CASPT2 and the corresponding CASSCF calculations always employed the same active spaces. For the DMRG calculations, the active spaces 1-5 in Table VII were chosen. The integrals were computed with the MOLPRO package[45] from natural orbitals generated from CASSCF calculations.

In the DMRG calculations, we have employed active spaces of two different sizes consisting of 32 and 44 active orbitals, respectively, and considered 32, 64, 100, 200, 400, 600, 800, and 1200 DMRG states. Up to 600 microiterations were required to achieve convergence of the energy. For all calculations, a level shift was applied in order to obtain pure singlet spin states as described above.

The relative energies of the $[Cu_2(\mu\text{-}\eta^2\text{:}\eta^2\text{-}O_2)]^{2+}$ and $[Cu_2(\mu\text{-}O)_2]^{2+}$ cores as well as of the $\{[(NH_3)_3Cu]_2(\mu\text{-}\eta^2\text{:}\eta^2\text{-}O_2)\}^{2+}$ and $\{[(NH_3)_3Cu]_2(\mu\text{-}O)_2\}^{2+}$ compounds are reliably produced by the DMRG algorithm for various numbers m of renormalized DMRG states and for different active spaces. The energy values for the active spaces 1-4 for structures **1** and **2** and for the active space 5 for **3** and **4** converge with increasing number of DMRG states. From Tables VIII–X it is apparent that DMRG calculations employing 32 DMRG states are not sufficient to obtain qualitatively correct energies. Note that the DMRG calculation for **2** using 200 DMRG states in active space 1 in Table VIII is an outlier and potentially trapped in a local minimum. This can be circumvented by starting the calculation by a different number of DMRG states and after a couple of sweeps switch back to the desired number of states.

To demonstrate the effect of adding random noise[15,19] to the reduced density matrix for the active subsystem (compare the discussion for CoH above), we reconsidered the DMRG(m=400) calculation of Table IX with CAS(32,44)

TABLE VII. Active spaces CAS(n,m) for the preparatory CASSCF calculation to produce the one-electron and two-electron integrals for the subsequent DMRG calculations. Doubly occupied orbitals are marked in bold face type. n and m are the number of electrons and orbitals, respectively. PG is an abbreviation for point group and BS for basis set. The different set numbers are denoted by 1–5. While 1–4 are valid for **1** and **2**, set 5 refers to **3** and **4**.

	n,m	PG	BS	Active space				
1	26,32	D_{2h}	BS1	$\mathbf{5}$–$\mathbf{7a_g}$	8–$10a_g$	$\mathbf{3b_{3u}}$	$4b_{3u}$	$\mathbf{3b_{2u}}$
				$\mathbf{4b_{2u}}$	5–$8b_{2u}$	$\mathbf{2b_{1g}}$	$3b_{1g}$	$\mathbf{3}$–$\mathbf{5b_{1u}}$
				6–$8b_{1u}$	$\mathbf{2b_{2g}}$	$3b_{2g}$	$\mathbf{2b_{3g}}$	3–$7b_{3g}$
				$\mathbf{1a_u}$	$2a_u$			
2	26,32	D_{2h}	BS1	$\mathbf{5}$–$\mathbf{7a_g}$	$8a_g$	$\mathbf{3b_{3u}}$	4–$6b_{3u}$	$\mathbf{3b_{2u}}$
				$\mathbf{4b_{2u}}$	$5b_{2u}$	$6b_{2u}$	$\mathbf{2b_{1g}}$	3–$5b_{1g}$
				$\mathbf{3}$–$\mathbf{5b_{1u}}$	$6b_{1u}$	$\mathbf{2b_{2g}}$	3–$5b_{2g}$	$\mathbf{2b_{3g}}$
				3–$5b_{3g}$	$\mathbf{1a_u}$	2–$4a_u$		
3	32,44	D_{2h}	BS2	$\mathbf{3}$–$\mathbf{7a_g}$	8–$12a_g$	$\mathbf{3b_{3u}}$	4–$5b_{3u}$	$\mathbf{2}$–$\mathbf{4b_{2u}}$
				5–$10b_{2u}$	$\mathbf{2b_{1g}}$	3–$5b_{1g}$	$\mathbf{2}$–$\mathbf{5b_{1u}}$	6–$10b_{1u}$
				$\mathbf{2b_{2g}}$	3–$4b_{2g}$	$\mathbf{2b_{3g}}$	3–$6b_{3g}$	$2a_u$
4	26,44	D_{2h}	BS2	$\mathbf{5}$–$\mathbf{7a_g}$	8–$10a_g$	$\mathbf{3b_{3u}}$	4–$7b_{3u}$	$\mathbf{2}$–$\mathbf{4b_{2u}}$
				5–$8b_{2u}$	$\mathbf{2b_{1g}}$	3–$6b_{1g}$	$\mathbf{3}$–$\mathbf{5b_{1u}}$	6–$8b_{1u}$
				$\mathbf{2b_{2g}}$	3–$6b_{2g}$	$\mathbf{2b_{3g}}$	3–$7b_{3g}$	$\mathbf{1a_u}$
				2–$5a_u$				
5	26,44	C_{2h}	BS3	$\mathbf{15}$–$\mathbf{18a_g}$	19–$25a_g$	$\mathbf{9}$–$\mathbf{11a_u}$	12–$19a_u$	$\mathbf{15}$–$\mathbf{17b_u}$
				18–$25b_u$	$\mathbf{8}$–$\mathbf{10a_g}$	11–$18a_g$		

TABLE VIII. Relative energies of **1** and **2** using basis set BS1.

Method	E_{bisoxo} (E_h)	E_{peroxo} (E_h)	ΔE (kJ mol^{-1})
	Active space 1 of Table VII		
DMRG(m=32)	−541.402 182 75	−541.135 398 69	−700.4
DMRG(m=64)	−541.432 367 69	−541.455 773 92	61.5
DMRG(m=100)	−541.434 525 92	−541.460 221 22	67.5
DMRG(m=200)	−541.413 739 57	−541.283 061 56	−343.1
DMRG(m=400)	−541.441 626 18	−541.461 944 65	53.3
DMRG(m=600)	−541.441 896 55	−541.462 061 95	52.9
	Active space 2 of Table VII		
DMRG(m=32)	−541.042 734 14	−541.026 908 67	−41.5
DMRG(m=64)	−541.434 307 98	−541.464 873 79	80.3
DMRG(m=100)	−541.446 934 32	−541.468 405 01	56.4
DMRG(m=200)	−541.448 185 60	−541.468 931 35	54.5
DMRG(m=400)	−541.460 475 74	−541.481 894 88	56.2
DMRG(m=600)	−541.460 876 73	−541.482 093 06	55.7
CASSCF(16,14)	−541.456 670 16	−541.453 589 46	−8.1
CASSCF(8,8)	−541.420 922 24	−541.375 104 16	−120.3
CASPT2(8,8)	−542.096 581 32	−542.133 350 13	96.5

active space 3 of Table VII and added 10^{-9} to the density matrix of the active subsystem. The energy decreased to −541.453 378 for the bis(μ-oxo) isomer and to −541.475 579 for the μ-η^2:η^2 peroxo isomer. That is, the energy is lowered in both cases but still far away from the DMRG reference obtained for large m. Nevertheless, the relative energy is 58.3 and thus remains almost constant when compared to the DMRG(m=400) energy difference of 59.1 in Table IX. Therefore, we do not apply the recipe advocated by Chan and co-workers[15,19] in the case of the copper clusters and rely instead on a comparison of results obtained for different values of m.

TABLE IX. Relative energies of **1** and **2** now using basis set BS2 and the active spaces 3 and 4 of Table VII.

Method	E_{bisoxo} (E_h)	E_{peroxo} (E_h)	ΔE (kJ mol^{-1})
	Active space 3 of Table VII		
DMRG(m=32)	−541.407 585 08	−541.222 570 67	−485.8
DMRG(m=64)	−541.431 214 32	−541.459 130 90	73.3
DMRG(m=100)	−541.439 834 93	−541.462 711 53	60.1
DMRG(m=200)	−541.442 855 87	−541.466 755 73	62.7
DMRG(m=400)	−541.452 932 51	−541.475 423 76	59.1
DMRG(m=600)	−541.453 651 24	−541.475 670 83	57.8
DMRG(m=800)	−541.453 984 02	−541.475 970 95	57.7
DMRG(m=1200)	−541.454 426 75	−541.476 144 71	57.0
	Active space 4 of Table VII		
DMRG(m=32)	−540.716 417 74	−541.060 185 09	902.6
DMRG(m=64)	−541.456 375 19	−541.479 968 62	61.9
DMRG(m=100)	−541.463 696 56	−541.494 473 08	80.8
DMRG(m=200)	−541.466 781 25	−541.496 679 80	78.5
DMRG(m=400)	−541.467 527 30	−541.497 171 27	77.8
DMRG(m=600)	−541.467 720 85	−541.497 274 43	77.6
DMRG(m=800)	−541.467 793 75	−541.497 314 24	77.5
CASSCF(16,14)	−541.467 083 19	−541.477 448 01	27.2
CASPT2(16,14)	−541.601 131 87	−541.598 756 46	−6.2
CASSCF(8,8)	−541.431 345 46	−541.425 640 59	−15.0
CASPT2(8,8)	−541.505 663 07	−541.510 177 90	11.9

TABLE X. Relative energies of **3** and **4** compounds using basis set BS3 active space 5 of Table VII for the DMRG calculations. The reference CASSCF and CASPT2 calculations were performed using BS2.

Method	E_{bisoxo} (E_h)	E_{peroxo} (E_h)	ΔE (kJ mol^{-1})
DMRG(m=32)	−878.938 533 93	−878.711 402 96	−596.3
DMRG(m=64)	−879.029 696 54	−879.097 431 80	177.8
DMRG(m=100)	−879.036 594 03	−879.100 232 65	167.1
DMRG(m=200)	−879.041 286 09	−879.101 377 78	157.8
DMRG(m=400)	−879.042 981 73	−879.101 746 90	154.3
DMRG(m=600)	−879.043 261 96	−879.102 003 98	154.2
DMRG(m=800)	−879.043 382 07	−879.102 043 41	154.0
CASSCF(16,14)	−879.275 988 03	−879.317 291 78	108.4
CASPT2(16,14)	−879.596 238 44	−879.632 776 38	95.9
CASSCF(8,8)	−879.211 171 85	−879.240 512 25	77.0
CASPT2(8,8)	−879.416 839 40	−879.318 770 56	−257.5

A comparison of the CASPT2 energies with those from the literature listed in Table V shows a qualitatively correct behavior in terms of energy differences, but the data show rather large deviations from each other. This can be mainly attributed to the different active spaces, which was already discussed by Rode and Werner.[63]

An important point to be discussed in the remainder of this section is the question whether the electronic energy of the two isomers is described with a comparable or even equal accuracy by the DMRG algorithm. Considering the incorporation of correlation effects in calculations on the bis(μ-oxo) and μ-η^2:η^2 peroxo structures, one understands from the CASSCF calculations that static electron correlation is more easily captured for the μ-η^2:η^2 peroxo cluster. Accordingly, the energy difference between the CASSCF and CASPT2 energy values is larger for the bis(μ-oxo) cluster. The fact that the electronic structure of the bis(μ-oxo) isomer is dominated by dynamical correlation effects while that of the μ-η^2:η^2 peroxo isomer is dominated by static electron correlation is also evident upon inspection of the CI coefficients in the CASSCF(8,8) and CASSCF(16,14) calculations which are given in Tables XI and XII. The wave function of the bis(μ-oxo) isomer is composed of more configurations with intermediate coefficients compared to the μ-η^2:η^2 peroxo isomer. By contrast, the electronic structure of the μ-η^2:η^2 peroxo isomer is mainly dominated by two configurations with large coefficients representing the singlet biradical character. The same qualitative results were already reported by Cramer *et al.*,[27,28] Rode and Werner,[63] and Flock and Pierloot.[62]

The DMRG energies are qualitatively agreeing with the reference energy values (see Table V). Quantitatively, however, it is very difficult to have a reliable basis for comparison because even the most sophisticated method, MRCI+Q, in Table V suffers from insufficiencies in the active space. Since in the DMRG calculations on **1** and **2**, the energy difference is comparable for various active spaces, one may assume that the results are reliable.

It is obvious from the absolute energy values of the μ-η^2:η^2 peroxo and bis(μ-oxo) isomers, in comparison to the CASSCF results with smaller CAS, that the total energies

TABLE XI. CI coefficients from the CASSCF(8,8)/BS2 and CASSCF(16,14)/BS2 calculations for **1** and **2** in D_{2h} symmetry. The occupation numbers indicate the occupation of the molecular orbitals in the corresponding active space. The orbitals can either be empty (0), doubly (2), or singly occupied with spin up (+) or spin down (−). The occupation numbers belonging to the same irreducible representation are grouped together.

	CASSCF(8,8)/BS2		CASSCF(16,14)/BS2	
Structure	Occupation no.	Coeff.	Occupation no.	Coeff.
1	20 20 20 20	0.739 770 5	2220 200 2220 200	0.721 680 5
	20 00 20 22	−0.362 595 6	2220 000 2220 220	−0.390 463 0
	00 22 20 20	−0.203 509 6	2200 220 2220 200	−0.226 757 7
	20 +− 20 −+	0.174 855 8	2220 −+0 2220 +−0	0.168 362 6
	20 −+ 20 +−	0.174 855 8	2220 +−0 2220 −+0	0.168 362 6
	20 −− 20 ++	−0.143 040 3	2220 −−0 2220 ++0	−0.129 844 0
	20 ++ 20 −−	−0.143 040 3	2220 ++0 2220 −−0	−0.129 844 0
	20 02 20 20	−0.125 151 1	2200 020 2220 220	0.113 539 1
	20 02 20 02	0.114 715 8	2220 020 2220 020	0.101 438 7
	20 20 20 02	−0.106 171 1		
	00 02 20 22	0.106 030 9		
2	20 20 20 20	0.784 061 8	2220 200 2220 200	0.815 489 1
	20 00 20 22	−0.578 967 9	2220 000 2220 220	−0.500 445 9
	00 22 20 20	−0.118 511 2	2200 220 2220 200	−0.116 441 4

of **3** and **4** are not fully converged. Nevertheless, the relative energy is obviously converged. With this result we arrive at the interesting observation that the relative energy of the different isomers can indeed be converged even if convergence has not been achieved for the total energy yet. Actually, we already observed this effect for the active space 1 in Table VIII. Here, the total energy of the bis(μ-oxo) isomer is above the CASSCF(16,14) reference energy, although the situation should be reversed because of the larger CAS in the DMRG calculation. Nevertheless, the energy difference of bis(μ-oxo) and μ-η^2:η^2 peroxo structures is already converged, as can be seen by comparison with the results obtained for the larger active space 2 given in the same table. Note also that the total energies of the larger CAS are now below the CASSCF(16,14) energies as they should be. The question arises how the relative energy can converge if the absolute energy is even found above a CASSCF energy with smaller CAS. Apparently, the DMRG calculation failed to pick up configurations in the renormalization step which are essential for a converged *total* energy. However, these con-

TABLE XII. CI coefficients in the CASSCF(8,8)/BS3 and CASSCF(16,14)/BS3 calculations for **3** and **4** in C_{2v} symmetry.

	CASSCF(8,8)/BS3		CASSCF(16,14)/BS3	
Structure	Occupation no.	Coeff.	Occupation no.	Coeff.
3	20 20 20 20	0.774 511 2	220 2200 220 2200	0.772 153 4
	20 00 20 22	−0.217 491 7	220 2000 220 2220	−0.200 869 8
	20 02 20 20	−0.188 642 6	220 2020 220 2200	−0.187 691 7
	20 −− 20 ++	0.164 081 5	220 2−−0 220 +2+0	0.162 155 2
	20 ++ 20 −−	0.164 081 5	220 2++0 220 −2−0	0.162 155 2
	20 −+ 20 +−	−0.145 524 0	220 2+−0 220 −2+0	−0.138 317 3
	20 +− 20 −+	−0.145 524 0	220 2−+0 220 +2−0	−0.138 317 3
	20 20 20 02	−0.135 762 2	220 2200 220 0220	−0.127 972 5
	00 22 20 20	−0.123 180 9	220 2+−0 220 2200	0.125 470 5
	20 02 20 02	0.122 831 0	220 2−+0 220 2200	−0.125 470 5
	20 −+ 20 20	−0.121 286 5	220 2020 220 0220	0.115 933 1
	20 +− 20 20	0.121 286 5	2+0 22−0 2+0 22−0	0.111 286 6
	+0 2− +0 2−	0.115 348 7	2−0 22+0 2−0 22+0	0.111 286 6
	−0 2+ −0 2+	0.115 348 7	200 2220 220 2200	−0.106 939 4
4	20 20 20 20	0.689 527 9	220 2200 220 2200	0.736 046 6
	20 00 20 22	−0.635 276 3	220 2000 220 2220	−0.624 539 9
	20 20 20 −+	−0.186 466 7	200 2220 220 2200	−0.112 007 7
	20 20 20 +−	0.186 466 7		
	00 22 20 20	−0.117 340 2		
	00 02 20 22	0.106 033 9		

figurations are obviously not important for the relative energy. Or to put it in other words, the energy contribution of the missing configurations would drop out upon subtracting the total energies of both isomers. In the CI framework this has been exploited to propose the so-called difference-dedicated CI model,[73,74] which aims at the construction of a CI wave function that comprises only electronic configurations relevant for an accurate energy *difference*.

Another peculiarity can be observed in Table VIII. This is the fact that the DMRG energy of the μ-η^2:η^2 peroxo isomer is indeed lower than the energy from the CASSCF(16,14) calculation [only the bis(μ-oxo) energy is above the smaller-CAS CASSCF(16,14) calculation]. This demonstrates why the CASSCF(16,14) yields a wrong relative energy of the two isomers since the CAS(16,14) is too small for the μ-η^2:η^2 peroxo isomer, while it is appropriate for the bis(μ-oxo) cluster. On the other hand, the large-CAS DMRG calculation collects all relevant electronic configurations of importance for the total state (in terms of large CI coefficients) in the renormalization steps (independent of the fact that the total energy is not converged). It is thus important to provide a larger CAS from which DMRG will pick the most important configurations so that balanced wave functions can be optimized for the different molecular structures of the cluster isomers.

To conclude, the energy differences between the bis(μ-oxo) and μ-η^2:η^2 peroxo structures can be reliably calculated for a given active space. This indicates that a further increase in the number of DMRG system states m—or an increase of the active space—will not change the results considerably. It is therefore possible to obtain an appropriate approximation to the energy difference for a relatively small number of renormalized DMRG system states. As expected, the DMRG algorithm is able to provide even better results than standard CASSCF calculations. However, as expected, the DMRG wave function is not able to entirely account for the dynamic electron correlation. This points to the need of a subsequent perturbation theory treatment to enhance the performance of the DMRG algorithm *a posteriori*.

V. CONCLUSION

In this work we have demonstrated the feasibility and accuracy of large-CAS DMRG calculations for the calculation of relative energies of transition-metal-containing molecules. Many quantum chemical methods have difficulties to describe transition metal compounds accurately. In the DMRG approach, however, we can consider a larger number of active orbitals in the calculation and, hence, molecules with a large amount of static electron correlation are well described by DMRG. In particular, we showed that the energy difference of states of different spin in CoH and NiCO as well as the energy difference of two different oxo-bridged copper complexes can be reliably converged within this CAS-CI-type DMRG approach.

DMRG has been validated for molecules with a small number of active orbitals, where CASSCF reference results could be reproduced exactly. However, we can afford a considerably larger number of active orbitals in the DMRG calculations than accessible by the standard CASSCF approach. Test calculations indicated that natural orbitals obtained from a preceding CASSCF calculation often lead to a lower total energy than Hartree-Fock orbitals in the DMRG calculations (see also Ref. 8), which is the reason why we have employed natural orbitals in all calculations on transition metal complexes.

DMRG total energies usually decrease monotonically with an increasing number of DMRG states m; one notices, however, outliers which converge to a local minimum with a too high energy. The outliers do not pose a problem since they can be easily identified and then excluded. For a better understanding, future work will be devoted to the analysis of these stationary points (local minima or saddle points) using the decomposition of DMRG states into a Slater determinant basis.[16] In all our calculations, we have found that the total energies as well as the relative energies converge to a certain value when the number of DMRG states m is increased. Even when the total energy values are not yet converged, the relative energies are almost constant in view of the chemical accuracy required, i.e., they are converged to about 1 kJ mol^{-1}.

Analyzing our results, we propose the following protocol for DMRG calculations on transition metal compounds. Natural orbitals are obtained from a preceding cheap CASSCF calculation, employing about 10–12 active orbitals. These natural orbitals are used in the DMRG calculation; the active space can easily comprise up to about 45 orbitals. As in CASSCF calculations, the active space has to be selected thoroughly, although the dependence of the result on the choice of the active space is much smaller than in CASSCF calculations and the selection is more straightforward since a much larger number of orbitals can be considered. If it is deemed necessary, several orbital orderings and adding random noise to the density matrix of the active subsystem may be checked in order to avoid convergence to a wrong local minimum or saddle point. A series of calculations with an increasing number of DMRG states m should be performed. If these calculations show a systematic decrease of the energy with increasing m, the obtained result can be considered reliable.

Every quantum chemical method has its particular strengths, which defines its niche for computational chemistry. It could be demonstrated in this work that one niche of DMRG will be the transition metal chemistry of open-shell complexes and clusters. DMRG is capable of producing CASSCF-type wave functions for electronic structures that require active spaces much larger than those that can be handled in a standard CASSCF calculation, i.e., for active spaces with more than 18 electrons in 18 spatial orbitals. Thus, DMRG can produce qualitatively correct large-scale CASSCF wave functions and energies. In future work, we plan to improve on these results by a subsequent perturbation theory treatment within the DMRG approach in order to capture the missing contributions of dynamic correlation effects in the same manner like CASPT2 improves on CASSCF results if the latter yields an appropriate and well-balanced reference wave function.

ACKNOWLEDGMENTS

This work was generously funded by the German Research Council DFG who continued funding (mainly through the Project Nos. Re1703/1-1 and Re1703/1-2) in Switzerland after the relocation of M.R. from Jena to Zurich. We are indebted to the DFG that this was made possible. We thank Professor Christopher Cramer and Professor Laura Gagliardi for drawing our attention to the interesting copper clusters as well as Professor Roland Lindh and Professor Garnet K.-L. Chan for discussions.

[1] S. R. White, Phys. Rev. Lett. **69**, 2863 (1992).
[2] S. R. White, Phys. Rev. B **48**, 10345 (1993).
[3] U. Schollwöck, Rev. Mod. Phys. **77**, 259 (2005).
[4] G. Fano, F. Ortolani, and L. Ziosi, J. Chem. Phys. **108**, 9246 (1998).
[5] S. R. White and R. L. Martin, J. Chem. Phys. **110**, 4127 (1999).
[6] S. Daul, I. Ciofini, C. Daul, and S. White, Int. J. Quantum Chem. **79**, 331 (2000).
[7] A. O. Mitrushenkov, G. Fano, F. Ortolani, R. Linguerri, and P. Palmieri, J. Chem. Phys. **115**, 6815 (2001).
[8] A. O. Mitrushenkov, R. Linguerri, P. Palmieri, and G. Fano, J. Chem. Phys. **119**, 4148 (2003).
[9] G. K.-L. Chan and M. Head-Gordon, J. Chem. Phys. **118**, 8551 (2003).
[10] G. K.-L. Chan, M. Kallay, and J. Gauss, J. Chem. Phys. **121**, 6110 (2004).
[11] G. K.-L. Chan, J. Chem. Phys. **120**, 3172 (2004).
[12] Ö. Legeza, J. Röder, and B. A. Hess, Phys. Rev. B **67**, 125114 (2003).
[13] Ö. Legeza, J. Röder, and B. A. Hess, Mol. Phys. **101**, 2019 (2003).
[14] Ö. Legeza and J. Sólyom, Phys. Rev. B **68**, 195116 (2003).
[15] G. K.-L. Chan and M. Head-Gordon, J. Chem. Phys. **116**, 4462 (2002).
[16] G. Moritz and M. Reiher, J. Chem. Phys. **126**, 244109 (2007).
[17] G. K.-L. Chan and T. Van Voorhis, J. Chem. Phys. **122**, 204101 (2005).
[18] J. Hachmann, W. Cardoen, and G. K.-L. Chan, J. Chem. Phys. **125**, 141101 (2006).
[19] J. J. Dorando, J. Hachmann, and G. K.-L. Chan, J. Chem. Phys. **127**, 084109 (2007).
[20] G. Moritz, A. Wolf, and M. Reiher, J. Chem. Phys. **123**, 184105 (2005).
[21] G. Moritz, B. A. Hess, and M. Reiher, J. Chem. Phys. **122**, 024107 (2005).
[22] G. Moritz and M. Reiher, J. Chem. Phys. **124**, 034103 (2006).
[23] L. Gagliardi and B. O. Roos, Chem. Soc. Rev. **36**, 893 (2007).
[24] H. P. Lüthi, J. Mol. Struct.: THEOCHEM **388**, 299 (1996).
[25] H. Koch, P. Jørgensen, and T. Helgaker, J. Chem. Phys. **104**, 9528 (1996).
[26] S. Coriani, A. Haaland, T. Helgaker, and P. Jørgensen, ChemPhysChem **7**, 245 (2006).
[27] C. J. Cramer, M. Włoch, P. Piecuch, C. Puzzarini, and L. Gagliardi, J. Phys. Chem. A **110**, 1991 (2006).
[28] C. J. Cramer, M. Włoch, P. Piecuch, C. Puzzarini, and L. Gagliardi, J. Phys. Chem. A **111**, 4871 (2007).
[29] R. Poli and J. N. Harvey, Chem. Soc. Rev. **32**, 1 (2003).
[30] J. N. Harvey, Struct. Bonding (Berlin) **112**, 151 (2004).
[31] F. Illas, I. Moreira, C. de Graaf, and V. Barone, Theor. Chem. Acc. **104**, 265 (2000).
[32] M. Reiher, O. Salomon, and B. A. Hess, Theor. Chem. Acc. **107**, 48 (2001).
[33] M. Reiher, Inorg. Chem. **41**, 6928 (2002).
[34] O. Salomon, M. Reiher, and B. A. Hess, J. Chem. Phys. **117**, 4729 (2002).
[35] M. Reiher, Faraday Discuss. **135**, 97 (2007).
[36] A. Fouqueau, S. Mer, M. E. Casida, L. M. L. Daku, A. Hauser, T. Mineva, and F. Neese, J. Chem. Phys. **120**, 9473 (2005).
[37] G. Ganzenmüller, N. Berkaine, A. Fouqueau, M. E. Casida, and M. Reiher, J. Chem. Phys. **122**, 234321 (2005).
[38] L. M. L. Daku, A. Vargas, A. Hauser, A. Fouqueau, and M. E. Casida, ChemPhysChem **6**, 1393 (2005).
[39] A. Fouqueau, M. E. Casida, L. M. L. Daku, A. Hauser, and F. Neese, J. Chem. Phys. **122**, 044110 (2005).
[40] S. Zein, S. A. Borshch, P. Fleurat-Lessard, M. E. Casida, and H. Chermette, J. Chem. Phys. **126**, 014105 (2007).
[41] H. Paulsen, L. Duelund, H. Winkler, H. Toftlund, and A. X. Trautwein, Inorg. Chem. **40**, 2201 (2001).
[42] E. R. Davidson, J. Comput. Phys. **17**, 87 (1975).
[43] J. S. Dewar, Bull. Soc. Chim. Fr. **18**, C71 (1951).
[44] J. Chatt and L. A. Duncanson, J. Chem. Soc. 2939 (1953).
[45] H.-J. Werner, P. J. Knowles, R. Lindh, M. Schütz *et al.*, MOLPRO, version 2002.6, a package of *ab initio* programs, 2002, see http://www.molpro.net
[46] T. H. Dunning, Jr., J. Chem. Phys. **90**, 1007 (1989).
[47] R. Kendall, T. H. Dunning, Jr., and R. J. Harrison, J. Chem. Phys. **96**, 6796 (1992).
[48] A. D. Becke, Phys. Rev. A **38**, 3098 (1988).
[49] J. P. Perdew, Phys. Rev. B **33**, 8822 (1986).
[50] A. D. Becke, J. Chem. Phys. **98**, 5648 (1993).
[51] C. Lee, W. Yang, and R. G. Parr, Phys. Rev. B **37**, 785 (1988).
[52] Ľ. Horný, A. Paul, Y. Yamaguchi, and H. F. Schaefer III, J. Chem. Phys. **121**, 1412 (2004).
[53] K. A. Magnus, H. Tonthat, and J. E. Carpenter, Chem. Rev. (Washington, D.C.) **94**, 727 (1994).
[54] E. I. Solomon, F. Tuczek, D. E. Root, and C. A. Brown, Chem. Rev. (Washington, D.C.) **94**, 827 (1994).
[55] L. M. Mirica, X. Ottenwaelder, and T. D. P. Stack, Chem. Rev. (Washington, D.C.) **104**, 1013 (2004).
[56] P. E. M. Siegbahn and M. R. A. Blomberg, Annu. Rev. Phys. Chem. **50**, 221 (1999).
[57] P. E. M. Siegbahn, Faraday Discuss. **124**, 289 (2003).
[58] J. A. Halfen, S. Mahapatra, E. C. Wilkinson, S. Kaderli, V. G. Young, L. Que, A. D. Zuberbühler, and W. B. Tolman, Science **271**, 1397 (1996).
[59] C. J. Cramer, B. A. Smith, and W. B. Tolman, J. Am. Chem. Soc. **118**, 11283 (1996).
[60] W. B. Tolman, Acc. Chem. Res. **30**, 227 (1997).
[61] S. Mahapatra, J. A. Halfen, E. C. Wilkinson, L. Que, and W. B. Tolman, J. Am. Chem. Soc. **116**, 9785 (1994).
[62] M. Flock and K. Pierloot, J. Phys. Chem. A **103**, 95 (1999).
[63] M. F. Rode and H.-J. Werner, Theor. Chem. Acc. **114**, 309 (2005).
[64] A. Volbeda and W. G. J. Hol, J. Mol. Biol. **209**, 249 (1989).
[65] K. A. Magnus, B. Hazes, H. Tonthat, C. Bonaventura, J. Bonaventura, and W. G. J. Hol, Proteins **19**, 302 (1994).
[66] R. Hoffmann, J. Chem. Phys. **39**, 1397 (1963).
[67] G. A. Landrum and W. V. Glassey, YAEHMOP extended Hückel molecular orbital package, see http://sourceforge.net/projects/yaehmop/
[68] K. Pierloot, in *Computational Organometallic Chemistry*, edited by T. R. Cundari (Dekker, New York, 2001), p. 123.
[69] M. Dolg, U. Wedig, H. Stoll, and H. Preuss, J. Chem. Phys. **2**, 866 (1986).
[70] K. Pierloot, B. Dumez, P.-O. Widmark, and B. O. Roos, Theor. Chim. Acta **90**, 87 (1995).
[71] P.-O. Widmark, P.-Å. Malmqvist, and B. Roos, Theor. Chim. Acta **77**, 291 (1990).
[72] T. H. Dunning, Jr., J. Chem. Phys. **53**, 2823 (1970).
[73] O. Castell, R. Caballol, and J. P. Malrieu, Chem. Phys. **172**, 33 (1993).
[74] F. Neese, J. Chem. Phys. **119**, 9428 (2003).